DOI: 10.1002/ejic.201100283

Rare-Earth Cobalt Gallides $RE_4Co_3Ga_{16}$ (RE = Gd–Er, Y): Self-Interstitial Derivatives of RE_2CoGa_8

Brianna R. Slater,[a] Haiying Bie,[a] Michael W. Gaultois,[a] Stanislav S. Stoyko,[a] and Arthur Mar*[a]

Dedicated to Professor John D. Corbett on the occasion of his 85th birthday

Keywords: Rare earths / Cobalt / Gallium / Intermetallic phases / Magnetic properties

Ternary rare-earth cobalt gallides $RE_4Co_3Ga_{16}$ (RE = Gd–Er, Y) have been prepared by arc-melting of the elements followed by annealing at 800 °C. Single crystals of the Gd and Tb members were also grown in the presence of a Ga self-flux. They extend the rare-earth substitution possible in the $Sm_4Co_3Ga_{16}$-type structure (Pearson symbol *tP*23, space group *P*4/*mmm*, *Z* = 1), in which additional Co atoms enter as self-interstitials into the parent RE_2CoGa_8 structure. Structural refinements were carried out on single-crystal (RE = Gd, Tb) and powder (RE = Dy, Ho, Er, Y) X-ray diffraction data. Cell parameters lie in the ranges of a = 6.03–5.96 Å and c = 11.11–10.96 Å. Magnetic measurements on $RE_4Co_3Ga_{16}$ (RE = Gd, Tb, Dy) reveal that they order antiferromagnetically below T_N of 19, 25, and 14 K, respectively; $Y_4Co_3Ga_{16}$ is Pauli paramagnetic. The electrical resistivity of $Tb_4Co_3Ga_{16}$ undergoes a transition coincident with the magnetic ordering temperature. Band structure calculations on $Y_4Co_3Ga_{16}$ indicate that the major bonding contributions arise from Co–Ga and Ga–Ga interactions, with the stuffing of interstitial Co atoms into octahedral sites of the parent Y_2CoGa_8 structure, which provides additional Co–Ga bonding stabilization.

Introduction

An emerging series of ternary intermetallic gallides and indides with tetragonal structures can be described by the general formula $RE_nM_mX_{3n+2m}$ (RE = rare-earth metal, mostly Ce and Yb; M = Co, Rh, Ir; X = Ga, In), in which the indices n and m refer to the number of $AuCu_3$-type and $PtHg_2$-type slabs, respectively, that are condensed together.[1–3] Although many hypothetical structures can be generated in this manner, $CePt_2In_7$ remains the only compound known with n = 1 and m = 2.[4] All other real examples are restricted to n = 1, 2 and m = 1; the general formula then simplifies to RE_nMX_{3n+2}. These compounds, especially $CeCoIn_5$,[5] have elicited considerable interest as heavy fermion materials and unconventional superconductors.[6–14] The n = 1 members, which are numerous, include the actinide superconductor $PuCoGa_5$ (T_c = 18 K);[15,16] the n = 2 members exhibit predominantly antiferromagnetic ordering and some also show superconductivity, such as Ce_2CoIn_8 (T_c = 0.4 K).[17] Among the rare-earth cobalt gallides RE_nCoGa_{3n+2}, previous magnetic studies have led to the observation that both the antiferromagnetic ordering temperatures and superconducting critical temperatures tend to decrease on proceeding from $RECoGa_5$ to RE_2CoGa_8.[8,11] Given these trends, an ongoing goal in these studies is to seek an understanding of how the physical properties correlate with, among other factors, the crystal structures, which are built up from such recognizable slabs.

In the course of investigating the Sm–Co–Ga system (motivated by the chemical similarity of Sm to Pu), Jia et al. recently discovered the superconducting compound $Sm_4Co_3Ga_{16}$ (T_c = 2.8 K).[18] This result highlights the possibility for further structural variation not evident from the formula RE_nMX_{3n+2}. The structure of $Sm_4Co_3Ga_{16}$ is derived by stuffing additional Co atoms into available octahedral sites within pairs of $REGa_3$ slabs of RE_2CoGa_8 (or "$RE_4Co_2Ga_{16}$"). Herein we explore the extent of RE substitution in the $Sm_4Co_3Ga_{16}$ structure, clarify the bonding with the aid of band structure calculations and examine the magnetic properties of some of these analogues.

Results and Discussion

Crystal Structure

The preparation of $RE_4Co_3Ga_{16}$ underscores the richness of the RE–Co–Ga systems, which already comprise many ternary intermetallic compounds.[19] The previously unique structure of $Sm_4Co_3Ga_{16}$[18] has now been extended

[a] Department of Chemistry, University of Alberta, Edmonton, AB T6G 2G2, Canada
Fax: +1-780-492-8231
E-mail: arthur.mar@ualberta.ca

Supporting information for this article is available on the WWW under http://dx.doi.org/10.1002/ejic.201100283.

to include representatives with the smaller RE metals (Gd–Er, Y); the cell parameters vary smoothly in this series (Figure 1). Synthesis of these compounds (through reaction of the elements by arc-melting followed by annealing at 800 °C) becomes more difficult with smaller RE elements, for which the samples contain other phases such as RE_2CoGa_8 with a closely related structure.[1] Crystals of $RE_4Co_3Ga_{16}$ and RE_2CoGa_8 are impossible to distinguish visually except by full single-crystal X-ray diffraction analysis. Fortunately, the Gd and Tb members could be obtained as single crystals through use of excess Ga as a self-flux. For the remaining members, powder X-ray diffraction data were refined with the Rietveld method. A representative fit to the diffraction pattern is shown for $Dy_4Co_3Ga_{16}$ in Figure 2; fits for the other compounds are available in Figure S1 in Supporting Information. Crystallographic data for all six compounds are summarized in Table 4, final values of the positional and displacement parameters are given in Table 1 and interatomic distances are given in Table 2.

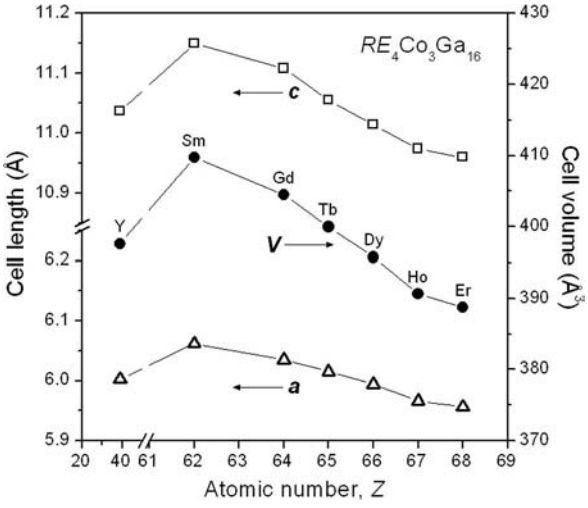

Figure 1. Plot of cell parameters for $RE_4Co_3Ga_{16}$.

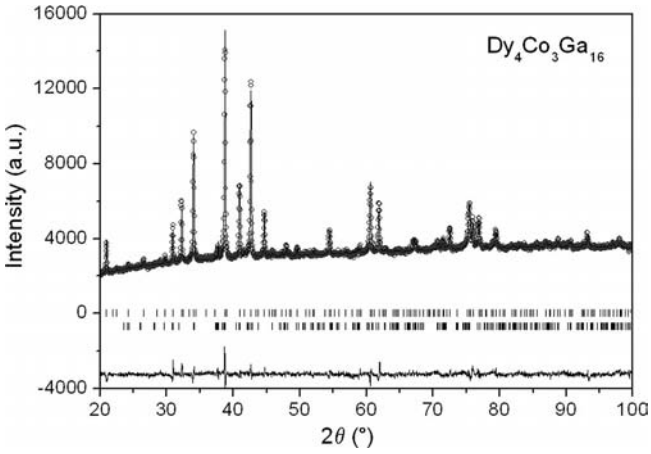

Figure 2. Rietveld refinement results for $Dy_4Co_3Ga_{16}$. The observed profile is indicated by circles and the calculated profile by the solid line. Bragg peak positions are located by the upper set of vertical tick marks; the lower set corresponds to small amounts (ca. 4%) of $Dy_2Co_3Ga_9$. The difference plot is shown at the bottom.

A $\sqrt{2}a \times \sqrt{2}a$ superstructure develops on proceeding from RE_2CoGa_8 to $RE_4Co_3Ga_{16}$. The *c*/*a* ratio in the RE_2CoGa_8 (RE = Sm, Gd–Tm, Lu, Y) series has a constant value of 2.61,[1,11] essentially identical to the $\sqrt{2}(c/a)$ ratio of $\sqrt{2} \times 1.84 = 2.60$ in the $RE_4Co_3Ga_{16}$ series (RE = Sm, Gd–Er, Y). Although the structure of $RE_4Co_3Ga_{16}$ is derived by stuffing Co atoms into the structure of RE_2CoGa_8, analysis

Table 1. Atomic coordinates and equivalent isotropic displacement parameters for $RE_4Co_3Ga_{16}$ (RE = Gd–Er, Y).[a]

	$Gd_4Co_3Ga_{16}$	$Tb_4Co_3Ga_{16}$	$Dy_4Co_3Ga_{16}$	$Ho_4Co_3Ga_{16}$	$Er_4Co_3Ga_{16}$	$Y_4Co_3Ga_{16}$
RE at 4*i* (0, $^1/_2$, *z*)						
z	0.19427(3)	0.19396(4)	0.1935(3)	0.1927(3)	0.1939(3)	0.1959(4)
U_{eq} or U_{iso} (Å^2)	0.0067(2)	0.0066(2)	0.015(2)	0.024(2)	0.007(2)	0.011(2)
Co1 at 2*e* (0, $^1/_2$, $^1/_2$)						
U_{eq} or U_{iso} (Å^2)	0.0072(3)	0.0069(4)	0.006(3)	0.004(3)	0.006(3)	0.036(4)
Co2 at 1*a* (0, 0, 0)						
U_{eq} or U_{iso} (Å^2)	0.0117(5)	0.0124(5)	0.006(3)	0.004(3)	0.006(3)	0.036(4)
Ga1 at 8*r* (*x*, *x*, *z*)						
x	0.24999(8)	0.25016(9)	0.252(1)	0.251(1)	0.251(2)	0.251(1)
z	0.38505(7)	0.38431(8)	0.3836(3)	0.3825(3)	0.3835(3)	0.3821(3)
U_{eq} or U_{iso} (Å^2)	0.0103(2)	0.0096(2)	0.011(1)	0.020(1)	0.016(2)	0.015(1)
Ga2 at 4*j* (*x*, *x*, 0)						
x	0.2809(1)	0.2805(2)	0.282(1)	0.273(1)	0.272(2)	0.283(1)
U_{eq} or U_{iso} (Å^2)	0.0102(2)	0.0104(2)	0.011(1)	0.020(1)	0.016(2)	0.015(1)
Ga3 at 2*h* ($^1/_2$, $^1/_2$, *z*)						
z	0.1952(1)	0.1954(2)	0.201(1)	0.211(2)	0.206(2)	0.200(1)
U_{eq} or U_{iso} (Å^2)	0.0099(3)	0.0090(3)	0.011(1)	0.020(1)	0.016(2)	0.015(1)
Ga4 at 2*g* (0, 0, *z*)						
z	0.2194(1)	0.2190(2)	0.223(1)	0.213(2)	0.214(2)	0.222(1)
U_{eq} or U_{iso} (Å^2)	0.0101(3)	0.0101(3)	0.011(1)	0.020(1)	0.016(2)	0.015(1)

[a] U_{eq}, defined as one-third of the trace of the orthogonalized U_{ij} tensor, applies to results from single-crystal data (RE = Gd, Tb); U_{iso} applies to results from powder Rietveld refinements (RE = Dy, Ho, Er, Y).

Table 2. Selected interatomic distances (Å) in $RE_4Co_3Ga_{16}$ (RE = Gd–Er, Y).

	$Gd_4Co_3Ga_{16}$	$Tb_4Co_3Ga_{16}$	$Dy_4Co_3Ga_{16}$	$Ho_4Co_3Ga_{16}$	$Er_4Co_3Ga_{16}$	$Y_4Co_3Ga_{16}$
RE–Ga1 (×4)	3.0071(6)	2.9917(7)	2.979(5)	2.964(6)	2.958(8)	2.954(5)
RE–Ga3 (×2)	3.0174(3)	3.0074(2)	2.998(1)	2.990(1)	2.981(1)	3.001(1)
RE–Ga4 (×2)	3.0302(3)	3.0200(3)	3.015(1)	2.991(1)	2.986(2)	3.015(1)
RE–Ga2 (×4)	3.0460(3)	3.0311(4)	3.018(5)	2.993(6)	2.997(7)	3.042(5)
Co1–Ga1 (×8)	2.4865(4)	2.4815(5)	2.477(5)	2.472(6)	2.463(8)	2.489(4)
Co2–Ga2 (×4)	2.397(1)	2.386(1)	2.39(1)	2.31(1)	2.29(1)	2.401(5)
Co2–Ga4 (×2)	2.436(2)	2.421(2)	2.46(1)	2.34(2)	2.34(2)	2.46(1)
Ga1–Co1 (×2)	2.4865(4)	2.4815(5)	2.477(5)	2.472(6)	2.463(8)	2.489(4)
Ga1–Ga1	2.554(2)	2.558(2)	2.564(5)	2.579(5)	2.554(5)	2.602(5)
Ga1–Ga4	2.818(1)	2.805(2)	2.77(1)	2.82(1)	2.81(2)	2.76(1)
Ga1–Ga3	3.000(1)	2.980(1)	2.91(1)	2.82(1)	2.86(2)	2.91(1)
Ga1–Ga1 (×2)	3.017(1)	3.005(1)	2.98(1)	2.97(1)	2.97(1)	2.99(1)
Ga1–Ga1 (×2)	3.018(1)	3.009(1)	3.02(1)	2.99(1)	2.98(1)	3.01(1)
Ga2–Co2	2.397(1)	2.386(1)	2.39(1)	2.31(1)	2.29(1)	2.401(5)
Ga2–Ga2 (×2)	2.645(2)	2.640(2)	2.62(1)	2.70(1)	2.71(1)	2.61(1)
Ga2–Ga3 (×2)	2.863(1)	2.855(2)	2.89(1)	3.00(2)	2.96(2)	2.88(1)
Ga3–Ga2 (×4)	2.863(1)	2.855(2)	2.89(1)	3.00(2)	2.96(2)	2.88(1)
Ga3–Ga1 (×4)	3.000(1)	2.980(1)	2.91(1)	2.82(1)	2.86(2)	2.91(1)
Ga4–Co2	2.436(2)	2.421(2)	2.46(1)	2.34(2)	2.34(2)	2.46(1)
Ga4–Ga1 (×4)	2.818(1)	2.805(2)	2.77(1)	2.82(1)	2.81(2)	2.76(1)

of numerous crystals provides no evidence for the occurrence of nonstoichiometry in which Co atoms partially occupy the interstitial sites, i.e. $RE_4Co_{2+x}Ga_{16}$ ($0 < x < 1$). The parent RE_2CoGa_8 structure is built up of pairs of $AuCu_3$-type slabs alternating with $PtHg_2$-type slabs stacked along the *c* direction, $^2_\infty[REGa_3] + ^2_\infty[REGa_3] + ^2_\infty[CoGa_2]$, with RE atoms in cuboctahedral (CN12) and Co atoms in cubic (CN8) coordination environments of the Ga atoms. The condensation of two $[REGa_3]$ slabs leads to octahedral Ga_6 clusters that are empty in RE_2CoGa_8, but *half* of which are centred by additional Co atoms (CN6) in $RE_4Co_3Ga_{16}$ (Figure 3). Occupation of *all* these sites is precluded by the generation of Co–Ga distances that would be too short (2.1–2.3 Å) relative to the sum of the metallic radii (Pauling R_1 values of 1.16 Å for Co and 1.25 Å for Ga).[20] Instead, the filled Ga_6 clusters expand to accommodate more reasonable Co–Ga distances of 2.3–2.4 Å (comparable to typical values such as those found in $CoGa_3$),[21] whereas the empty Ga_6 clusters shrink considerably such that the centre-to-vertex distances become 1.9–2.2 Å [the shortest Co–Ga distance found in the literature is 2.195(4) Å in $YCoGa_3Ge$].[22] The constraint that the Co–Ga distances within these clusters do not become shorter than ca. 2.3 Å sets the limit of substitution with the smallest RE metal to $Er_4Co_3Ga_{16}$, even though the parent RE_2CoGa_8 structure extends all the way to the Lu member.[1,11] On the other hand, it might be thought that expansion of the structure by substitution with a larger RE metal should not be limited. For this consideration, it is important to note that the RE-centred cuboctahedra (in the $AuCu_3$-type slabs) share a common square face of Ga atoms with the Co-centred cubes (in the $PtHg_2$-type slabs). Because the $PtHg_2$-type slabs remain unperturbed on proceeding from RE_2CoGa_8 to $RE_4Co_3Ga_{16}$, the limit of substitution with the largest RE metal is the same for both series, at the Sm member. Within the range of RE substitution, the Ga–Ga distances within these squares (3.0 Å) match well with the RE–Ga

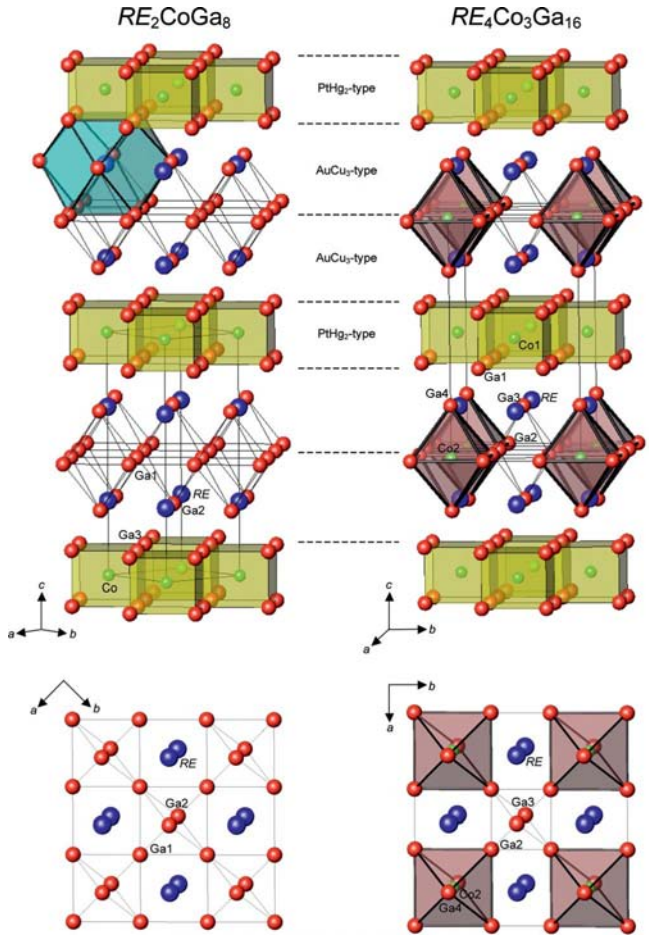

Figure 3. Comparison of RE_2CoGa_8 (RE = Sm, Gd–Tm, Lu, Y) and $RE_4Co_3Ga_{16}$ (RE = Sm, Gd–Er, Y) structures built up from $AuCu_3$- and $PtHg_2$-type slabs. The Co-centred cubes, as well as one of the RE-centred cuboctahedra, are highlighted in RE_2CoGa_8. Half of the formerly empty octahedral Ga_6 clusters in RE_2CoGa_8 are filled by additional Co atoms to form the structure of $RE_4Co_3Ga_{16}$.

distances (3.0 Å) to minimize distortion of the cub-octahedra. The Ga–Ga distances within the expanded Ga_6 clusters are longer (3.2–3.4 Å) and are nonbonding.

Properties

Measurements of the magnetic susceptibility reveal antiferromagnetic ordering at low temperatures for $RE_4Co_3Ga_{16}$ (RE = Gd, Tb, Dy) and temperature-independent Pauli paramagnetism for $Y_4Co_3Ga_{16}$ (Figure 4). For the Gd, Tb and Dy members, the inverse magnetic susceptibility was fitted to the Curie–Weiss law, $\chi = C/(T - \theta_p)$, in the linear portion of the high-temperature paramagnetic regime, and yielded the parameters listed in Table 3. The effective magnetic moments (derived from the Curie constants, C) slightly exceed the theoretical free-ion values for RE^{3+} species, but caution should be exercised because the samples contained small amounts of other phases which are magnetic (Figure S2 in Supporting Information). For example, the $Tb_4Co_3Ga_{16}$ sample contained ca. 3.5% by mass of $Tb_2Co_3Ga_9$.[23] In principle, it should be possible to subtract the contribution of these other phases from the total magnetic susceptibility, but unfortunately the magnetic properties of $RE_2Co_3Ga_9$ phases are unknown.[23] The contamination of the $Dy_4Co_3Ga_{16}$ sample with minor amounts of both $DyCoGa_5$ and $Dy_2Co_3Ga_9$ is probably responsible for the high effective magnetic moment observed. Alternatively, the elevated magnetic moments may be intrinsic to the compounds, possibly from the contribution of Co atoms. However, this explanation is unlikely because $Y_4Co_3Ga_{16}$, which contains a non-magnetic RE^{3+} ion, is Pauli paramagnetic (Figure 4d).

The magnetic behaviour of $RE_4Co_3Ga_{16}$ closely resembles that of the RE_2CoGa_8 phases, which also order antiferromagnetically at low temperatures.[10–14] The general trend is that the Néel temperatures, T_N, decrease on proceeding from RE_2CoGa_8 (20, 28 and 18 K)[11] to $RE_4Co_3Ga_{16}$ (19, 25 and 14 K) for the Gd, Tb and Dy members, respectively. Typical for ternary gallides or indides with related structures, such as those described in the introduction, RKKY interactions are assumed to be operative between the RE atoms. The values for T_N for $RE_4Co_3Ga_{16}$ roughly follow de Gennes scaling, with similar deviations seen for the Tb and Dy members as for the RE_2CoGa_8 series.[11] Many of the interesting metamagnetic transitions, characterized by steplike features seen in the isothermal magnetization curves for Tb_2CoGa_8 and Dy_2CoGa_8,[11] become much less pronounced or disappear al-

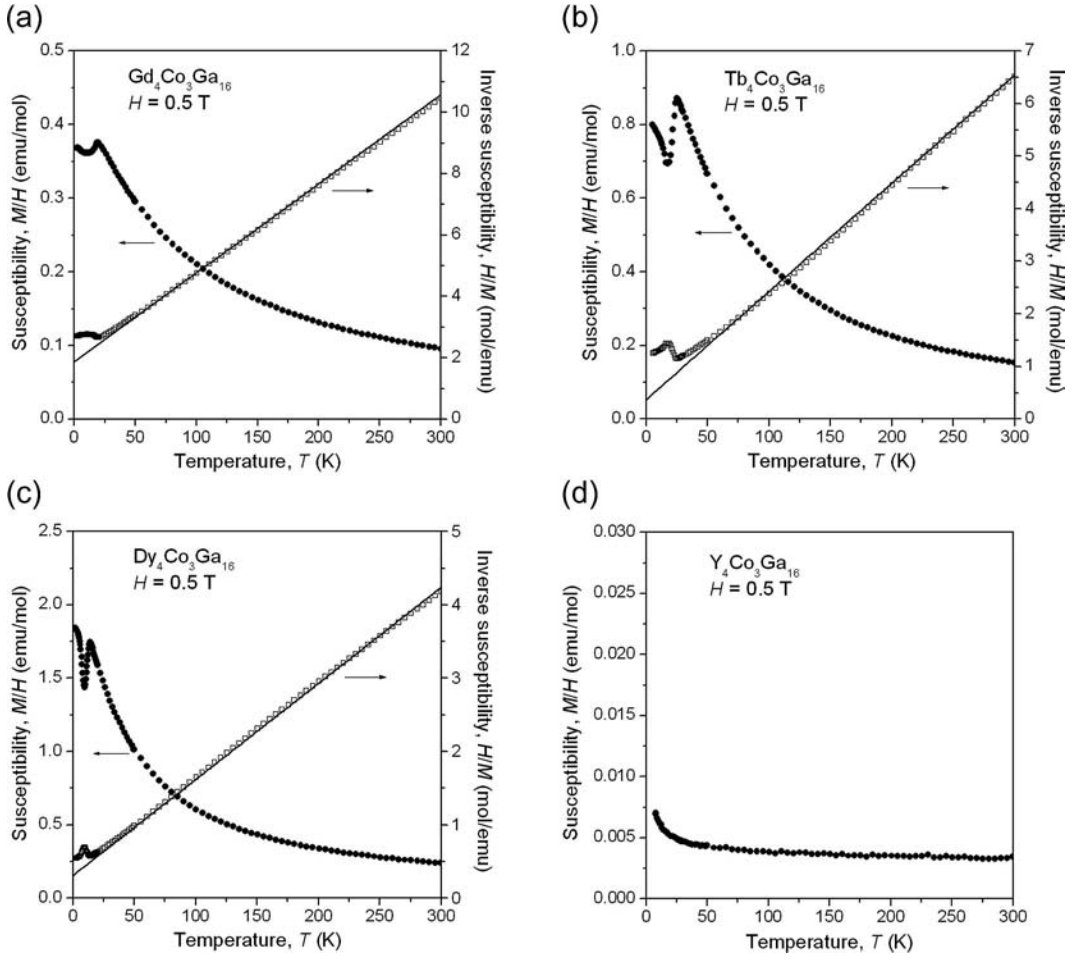

Figure 4. Zero-field-cooled dc magnetic susceptibility for $RE_4Co_3Ga_{16}$ (RE = Gd, Tb, Dy, Y). For the Gd, Tb and Dy members, the inverse susceptibility is also shown, fitted to the Curie–Weiss law.

Table 3. Summary of magnetic data for $RE_4Co_3Ga_{16}$ (RE = Sm, Gd, Tb, Dy, Y).

Compound	Behaviour	T_N (K)	θ_p (K)	$\mu_{eff,\ meas}$ (μ_B/RE)	$\mu_{eff,\ theor}$ for RE^{3+} (μ_B)
$Sm_4Co_3Ga_{16}$[a]	paramagnetic above 3.5 K			0.68	0.84
$Gd_4Co_3Ga_{16}$	antiferromagnetic	19	–65(1)	8.30(2)	7.94
$Tb_4Co_3Ga_{16}$	antiferromagnetic	25	–18(1)	9.85(2)	9.72
$Dy_4Co_3Ga_{16}$	antiferromagnetic	14	–24(1)	12.36(2)	10.64
$Y_4Co_3Ga_{16}$	Pauli paramagnetic				0

[a] Ref.[18] The measured value of μ_{eff} for $Sm_4Co_3Ga_{16}$ is 1.36 μ_B/f.u. or 0.68 μ_B/Sm (not 0.34 μ_B/Sm as erroneously reported because μ_{eff} must be divided by the square root of the number of Sm atoms).

together in the corresponding $Tb_4Co_3Ga_{16}$ and $Dy_4Co_3Ga_{16}$ compounds (Figure S3 in Supporting Information). This observation supports the proposal that crystalline electric field (CEF) effects experienced by the Tb or Dy atoms are responsible for the deviation in T_N from de Gennes scaling,[11] since the cuboctahedral coordination environment of Ga atoms around the RE atoms is distorted by the insertion of the interstitial Co2 atoms into the parent RE_2CoGa_8 structure to form $RE_4Co_3Ga_{16}$.

The electrical resistivity of a single-crystal sample of one member, $Tb_4Co_3Ga_{16}$, was measured (Figure 5). As the temperature is lowered, the resistivity decreases in a relatively linear fashion. This is followed by a more rapid drop below a kink at 25 K, which coincides with T_N in the magnetic susceptibility curve, consistent with the loss of spin-disorder scattering upon the onset of antiferromagnetic ordering. The behaviour is similar to that seen for Tb_2CoGa_8 and other RE_2CoGa_8 compounds.[10–12] No superconducting transition could be detected down to ca. 5 K.

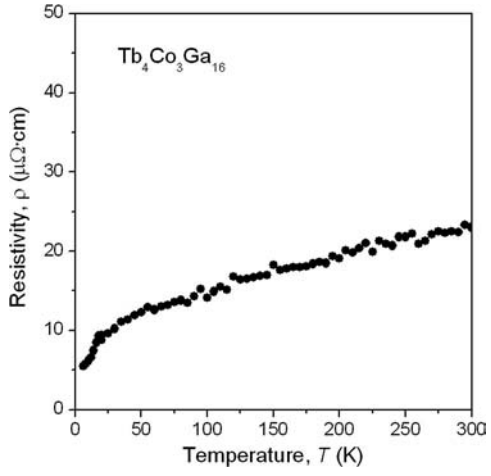

Figure 5. Electrical resistivity of $Tb_4Co_3Ga_{16}$ single crystal.

Electronic Structure

The electronic band structure was calculated for the nonmagnetic representative $Y_4Co_3Ga_{16}$. The density of states (DOS) curve (Figure 6a) resembles that previously determined for $Sm_4Co_3Ga_{16}$;[18] the Fermi level falls in a local minimum, consistent with the temperature-independent Pauli paramagnetism observed for $Y_4Co_3Ga_{16}$. The occurrence of mostly empty Y states, mostly filled Co states and partially filled Ga states agrees with the expected directions of electron transfer from the Y atoms to the more electronegative Co and Ga atoms. However, inspection of the crystal orbital Hamilton population (COHP) curves (Figure 6b) reveals that the bonding is far from ionic, given that the Y 5s/4d and Ga 4s/4p states mix over a wide energy range. Although these Y–Ga interactions are not strong (0.67 eV/bond), there are many of them because of the high CN12 coordination environments around the Y atoms. The most significant bonding contributions are the Co–Ga (2.4–2.5 Å, 1.88 eV/bond) and, to a lesser extent, the more distant Ga–Ga interactions (2.6–3.0 Å, 0.82 eV/bond). Interestingly, these Co–Ga and Ga–Ga interactions are precisely optimized, with bonding levels just completely occupied up to the Fermi level, a characteristic feature of Zintl phases. Notwithstanding the essentially identical Pauling electronegativities (1.8) of Co and Ga,[20] the nearly electron-precise formulation $(Y^{3+})_4(Co^{2+})_3(Ga^{1.1-})_{16}$ allows the prediction of weak multicentre polyanionic Ga–Ga bonding. Although the filled Co 3d states are found in a fairly narrow energy range (down to –4 eV below the Fermi level), they do not represent localized electrons. A spin-polarized LMTO calculation (not shown) attempted on $Y_4Co_3Ga_{16}$ confirms that no magnetic moments develop on any atom; this result rules out the contribution of Co atoms to the effective magnetic moments of the other $RE_4Co_3Ga_{16}$ members.

Because the structure of $RE_4Co_3Ga_{16}$ is derived from the RE_2CoGa_8 host structure, which has to be distorted to accommodate the self-interstitial Co atoms into the centres of the octahedral Ga_6 clusters, it is of interest to determine how the bonding interactions evolve. A band structure calculation performed on Y_2CoGa_8 (Figure S4 in Supporting Information) reveals a DOS curve that is similar to that of $Y_4Co_3Ga_{16}$. The most important difference is that the inclusion of the octahedrally coordinated Co interstitial atoms, whose 3d states clearly separate into crystal-field split t_{2g} and e_g sets (shaded region in the Co projection shown in Figure 6a), augments the total Co–Ga bonding. Within the cubes of the $PtHg_2$-type slabs, the Co–Ga bonding is essentially unchanged on progressing from Y_2CoGa_8 (1.84 eV/bond) to $Y_4Co_3Ga_{16}$ (1.82 eV/bond), but within the octahedra of the $AuCu_3$-type slabs, the newly inserted Co atoms provide an additional contribution of 1.94 eV/bond. The distortion elongates some Ga–Ga distances but shortens others within the Ga square net in the $AuCu_3$-type slabs (Figure 3) such that the overall Ga–Ga bonding is also little changed in Y_2CoGa_8 (0.78 eV/bond) and $Y_4Co_3Ga_{16}$ (0.82 eV/bond). The development of these favourable Co–

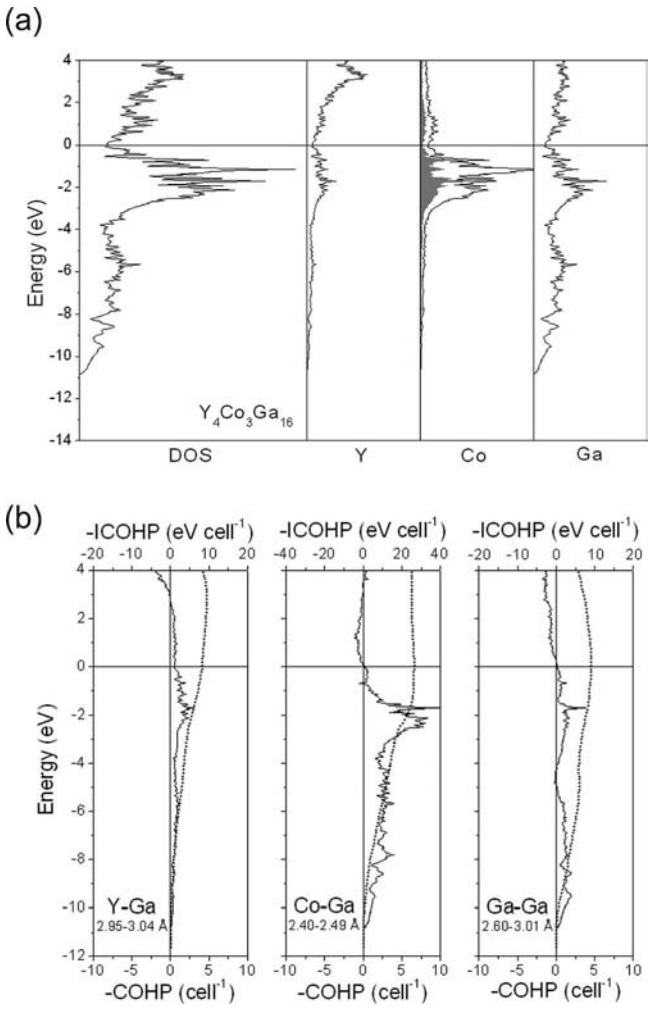

Figure 6. (a) Density of states (DOS) and its Y, Co and Ga projections for $Y_4Co_3Ga_{16}$. The shaded region in the Co projection highlights the contribution of the interstitial Co atoms centred within the octahedral Ga_6 clusters. (b) Crystal orbital Hamilton population (COHP) (solid line) and integrated COHP curves (dotted line) for Y–Ga, Co–Ga and Ga–Ga interactions. The horizontal lines at 0 eV mark the Fermi level.

Ga and Ga–Ga bonding interactions more than compensates for the weakening of the Y–Ga interactions (from 0.85 eV/bond in Y_2CoGa_8 to 0.67 eV/bond in $Y_4Co_3Ga_{16}$) as the Y-centred cuboctahedra distort to lower symmetry.

Conclusions

The preparation of $RE_4Co_3Ga_{16}$ demonstrates that the available sites at the centres of octahedral Ga_6 clusters in the parent RE_2CoGa_8 compounds (Ho_2CoGa_8-type structure) can be occupied by self-interstitial Co atoms, driven by a gain in additional Co–Ga bonding interactions. Structural considerations limit the extent of this series to the smaller RE atoms. It would be worthwhile to target the preparation of hypothetical $RE_4M_3Ga_{16}$ (M = Rh, Ir) or $RE_4Co_3In_{16}$ compounds to verify the factors limiting the substitutional range of RE. Analysis of the electronic structure suggests that, as in many other ternary RE–M–Ga phases,[24] electron transfer takes place from RE to both Co and Ga atoms, so that $RE_4Co_3Ga_{16}$ contains formally anionic Co species as well as a polyanionic Ga–Ga network with weak multicentre bonding. The distortion accompanying the stuffing of Co atoms into RE_2CoGa_8 tends to be detrimental to the occurrence of interesting physical properties; the magnetic ordering temperatures decrease slightly and no superconducting transition was observed down to ca. 5 K in $Tb_4Co_3Ga_{16}$. This observation continues the trend previously made about the relationship between local structural distortions around the RE atoms and the occurrence of magnetic ordering in $REMX_5$ and RE_2MX_8 compounds.[25]

Experimental Section

Synthesis: The starting materials were pieces of RE (Gd–Er, Y, 99.9%, Hefa), Co (99.5%, Aldrich) and Ga (99.99%, Cerac). These pieces were combined in stoichiometric proportions (4 RE + 3 Co + 16 Ga) and arc-melted in a Centorr 5TA tri-arc furnace or an Edmund Bühler MAM-1 compact arc melter on a water-cooled copper hearth under an argon atmosphere in the presence of a Ti getter. The alloys were melted, flipped over and remelted to ensure homogeneity; any weight loss was found to be less than 1%. The ingots were then sealed within evacuated fused-silica tubes and annealed at 800 °C for three weeks, followed by quenching in cold water. Attempts to extend the substitution to other RE metals (besides the previously known Sm member), both early and late, were unsuccessful under the same synthetic conditions.

Single crystals of the Gd and Tb members were obtained by combining excess Ga (0.3 g), which acts as a flux, with arc-melted ingots (0.3 g) prepared as described above and placed within fused-silica tubes, which were evacuated and sealed. The tubes were heated to 800 °C for two weeks, cooled to 500 °C over 48 h and then cooled to room temperature over 24 h. Black plate-shaped crystals were isolated from the Ga flux by sonication in warm ethanol, followed by filtration. Energy-dispersive X-ray (EDX) analysis of these crystals on a Hitachi S-2700 scanning electron microscope or a JEOL JSM 6700F field-emission scanning electron microscope revealed average compositions [atomic percentages of 19(2)% RE, 14(2)% Co and 67(2)% Ga] consistent with expectations (17% RE, 13% Co, 70% Ga). However, the uncertainties in this semiquantitative EDX analysis do not permit sufficient discrimination from related phases of similar composition, especially $RECoGa_5$ (14% RE, 14% Co, 71% Ga) and RE_2CoGa_8 (18% RE, 9% Co, 73% Ga). Moreover, these different phases crystallize with indistinguishable habits. The ultimate composition was established from the structure refinements described below. Extension of this crystal growth procedure to the other RE members (RE = Dy–Er, Y) yielded only crystals of $RECoGa_5$ and RE_2CoGa_8 when they were screened by single-crystal X-ray diffraction.

Structure Determination: Single-crystal X-ray diffraction data for $RE_4Co_3Ga_{16}$ (RE = Gd, Tb) were collected on a Bruker Platform/SMART 1000 CCD diffractometer at 22 °C by using ω scans (see Table 4). Structure solution and refinement were carried out with use of the SHELXTL (version 6.12) program package.[26] Face-indexed numerical absorption corrections were applied. The centrosymmetric tetragonal space group *P*4/*mmm* was chosen on the basis of intensity statistics and the isotypy with $Sm_4Co_3Ga_{16}$.[18] Initial atomic positions found by direct methods were consistent with $Sm_4Co_3Ga_{16}$; in particular, the interstitial Co2 atoms located at the

Table 4. Crystallographic data for $RE_4Co_3Ga_{16}$ (RE = Gd–Er, Y).[a]

	$Gd_4Co_3Ga_{16}$	$Tb_4Co_3Ga_{16}$	$Dy_4Co_3Ga_{16}$	$Ho_4Co_3Ga_{16}$	$Er_4Co_3Ga_{16}$	$Y_4Co_3Ga_{16}$
Formula mass (amu)	1921.31	1927.99	1942.32	1952.03	1961.35	1647.99
a (Å)	6.0348(5)	6.0147(4)	5.9940(3)	5.9662(2)	5.9557(3)	6.0020(3)
c (Å)	11.1073(10)	11.0555(8)	11.0143(6)	10.9740(4)	10.9598(5)	11.0369(5)
V (Å^3)	404.51(6)	399.95(5)	395.73(3)	390.62(2)	388.75(3)	397.59(3)
$\rho_{calcd.}$ (g cm^{-3})	7.887	8.005	8.150	8.298	8.378	6.883
Radiation	Mo-K_α	Mo-K_α	Cu-$K_{\alpha1}$	Cu-$K_{\alpha1}$	Cu-$K_{\alpha1}$	Cu-$K_{\alpha1}$
	λ = 0.71073 Å	λ = 0.71073 Å	λ = 1.54051 Å	λ = 1.54051 Å	λ = 1.54051 Å	λ = 1.54051 Å
μ (mm^{-1})	45.20	46.81	151.63	89.10	91.59	71.04
2θ range (°)	3.66–66.28	6.78–66.24	10.00–100.00	10.00–100.00	10.00–100.00	10.00–100.00
Refinement method	SHELXTL	SHELXTL	Rietveld	Rietveld	Rietveld	Rietveld
No. of data collected	5543	5554	3914	3914	3914	3914
No. of unique data	514 (R_{int} = 0.052) [483 with $F_o^2 > 2\sigma(F_o^2)$]	512 (R_{int} = 0.059) [492 with $F_o^2 > 2\sigma(F_o^2)$]	213[b]	209[b]	207[b]	212[b]
No. of variables	27	27	30	37	33	32
Residuals[c]	$R(F)$ [$F_o^2 > 2\sigma(F_o^2)$] = 0.024 $R_w(F_o^2)$ = 0.071	$R(F)$ [$F_o^2 > 2\sigma(F_o^2)$] = 0.031 $R_w(F_o^2)$ = 0.084	R_B = 0.095 R_p = 0.021 R_{wp} = 0.028	R_B = 0.092 R_p = 0.029 R_{wp} = 0.047	R_B = 0.085 R_p = 0.041 R_{wp} = 0.056	R_B = 0.100 R_p = 0.033 R_{wp} = 0.046

[a] Space group *P4/mmm* (No. 123); Z = 1. [b] Bragg reflections. [c] $R(F) = \Sigma||F_o| - |F_c||/\Sigma|F_o|$; $R_w(F_o^2) = \{\Sigma[w(F_o^2-F_c^2)^2]/\Sigma wF_o^4\}^{1/2}$, $w^{-1} = [\sigma^2(F_o^2) + (Ap)^2 + Bp]$ where $p = [\max(F_o^2,0) + 2F_c^2]/3$; $R_B = \Sigma|I_o-I_c|/\Sigma I_o$; $R_p = \Sigma|y_o - y_c|/\Sigma y_o$; $R_{wp} = [\Sigma[w(y_o - y_c)]/\Sigma wy_o^2]^{1/2}$.

origin were quite evident. Refinements proceeded in a straightforward manner; all sites were fully occupied with reasonable displacement parameters. Atomic positions were standardized with the program STRUCTURE TIDY.[27] Further details on the crystal structure investigations may be obtained from the Fachinformationszentrum Karlsruhe, 76344 Eggenstein-Leopoldshafen, Germany (fax: +49-7247-808-666; e-mail: crysdata@fiz-karlsruhe.de), on quoting the depository number CSD-422805 ($Gd_4Co_3Ga_{16}$) and -422806 ($Tb_4Co_3Ga_{16}$).

Powder X-ray diffraction data for $RE_4Co_3Ga_{16}$ (RE = Dy, Ho, Er, Y) were collected with Cu-$K_{\alpha1}$ radiation on an Inel powder diffractometer equipped with a CPS 120 detector and were refined with the full-profile Rietveld method with use of the program FullProf (version 4.80).[28] The least-squares refinements included scale factor, background, zero point, cell parameters, pseudo-Voigt peak profile parameters, atomic coordinates and isotropic displacement parameters. The displacement parameters were constrained to be equal for the two Co sites, and similarly for the four Ga sites. One reason for the relatively high R_B values is the likelihood that some RE_2CoGa_8 may be present as a minor impurity phase, as suggested by slight broadening of the peaks. All peaks in the powder diffraction pattern of RE_2CoGa_8 nearly overlap with those in $RE_4Co_3Ga_{16}$, which is distinguished mainly by the occurrence of additional weak superstructure peaks. However, the inability to resolve peaks belonging to RE_2CoGa_8 vs. $RE_4Co_3Ga_{16}$ (cf. $\sqrt{2}a$ = 5.97 Å, c = 10.99 Å for Ho_2CoGa_8 vs. a = 5.97 Å, c = 10.97 Å for $Ho_4Co_3Ga_{16}$) causes the refinements to be unstable if both phases are included. Uncorrected absorption effects also influence the quality of the refinements.

Magnetic Susceptibility and Electrical Resistivity: Bulk samples of $RE_4Co_3Ga_{16}$ were difficult to prepare in high purity. As ascertained by powder X-ray diffraction, four samples (RE = Gd, Tb, Dy, Y) could be obtained in adequate purity (less than ca. 3% by mass of other phases; Figure S2 in Supporting Information), whereas the remaining two samples (RE = Ho, Er) were not sufficiently pure (>10% of other phases) to permit bulk magnetic measurements. Measurements of dc magnetic susceptibility were made under an applied field of 5000 Oe on a Quantum Design 9T–PPMS dc magnetometer. The susceptibility was corrected for contributions from the holder and underlying sample diamagnetism.

Electrical resistivity measurements were attempted on numerous single-crystal samples, but these efforts were thwarted by the impossibility in distinguishing between crystals of $RE_4Co_3Ga_{16}$ and RE_2CoGa_8 by visual inspection or EDX analyses alone. Selected crystals of $Tb_4Co_3Ga_{16}$ were the only ones that could be obtained in sufficiently large size (0.3 to 0.8 mm in length) and whose identities could be verified individually as the desired compound by single-crystal X-ray diffraction analysis. The electrical resistivity was measured by standard four-probe methods on a Quantum Design PPMS system equipped with an ac transport controller (Model 7100). The current was 100 μA, and the frequency was 16 Hz.

Band Structure Calculations: Tight-binding linear muffin tin orbital (TB-LMTO) band structure calculations were performed on $Y_4Co_3Ga_{16}$ within the local density and atomic spheres approximation with use of the Stuttgart TB-LMTO program.[29] The basis sets consisted of Y 5s/5p/4d/4f, Co 4s/4p/3d and Ga 4s/4p/4d orbitals, and the Y 5p/4f and Ga 4d orbitals were downfolded. Integrations in reciprocal space were carried out with an improved tetrahedron method over 112 irreducible k points. For comparison, an analogous calculation was performed on Y_2CoGa_8, with atomic positions taken from the structure of Ho_2CoGa_8[1] and integrations carried out over 220 irreducible k points.

Supporting Information (see also the footnote on the first page of this article): Rietveld refinement results, powder XRD patterns, additional magnetic data, and density of states (for a calculation on Y_2CoGa_8) are presented.

Acknowledgments

This work was supported by the Natural Sciences and Engineering Research Council of Canada. We thank Dr. Robert McDonald and Dr. Michael J. Ferguson (X-ray Crystallography Laboratory) for assistance with the single-crystal X-ray data collection and Ms. Christina Barker (Department of Chemical and Materials Engineering) and Ms. De-Ann Rollings (Department of Earth and Atmospheric Sciences) for the EDX analyses.

[1] Yu. N. Grin', Ya. P. Yarmolyuk, E. I. Gladyshevskii, *Sov. Phys. Crystallogr.* **1979**, *24*, 137–139; Yu. N. Grin', Ya. P. Yarmolyuk, E. I. Gladyshevskii, *Transl. Kristallografiya* **1979**, *24*, 242–246.

[2] Ya. M. Kalychak, V. I. Zaremba, V. M. Baranyak, V. A. Bruskov, Yu. P. Zavalij, *Izv. Akad. Nauk SSSR Met.* **1989**, 209–210.
[3] Ya. M. Kalychak, *J. Alloys Compd.* **1999**, *291*, 80–88.
[4] Zh. M. Kurenbaeva, E. V. Murashova, Yu. D. Seropegin, H. Noël, A. I. Tursina, *Intermetallics* **2008**, *16*, 979–981.
[5] M. Kenzelmann, Th. Strässle, C. Niedermayer, M. Sigrist, B. Padmanabhan, M. Zolliker, A. D. Bianchi, R. Movshovich, E. D. Bauer, J. L. Sarrao, J. D. Thompson, *Science* **2008**, *321*, 1652–1654.
[6] P. G. Pagliuso, J. D. Thompson, M. F. Hundley, J. L. Sarrao, Z. Fisk, *Phys. Rev. B* **2001**, *63*, 054426–1–054426–4.
[7] R. T. Macaluso, J. L. Sarrao, P. G. Pagliuso, N. O. Moreno, R. G. Goodrich, D. A. Browne, F. R. Fronczek, J. Y. Chan, *J. Solid State Chem.* **2002**, *166*, 245–250.
[8] J. Hudis, R. Hu, C. L. Broholm, V. F. Mitrović, C. Petrovic, *J. Magn. Magn. Mater.* **2006**, *307*, 301–307.
[9] D. A. Joshi, C. V. Tomy, S. K. Malik, *J. Phys.: Condens. Matter* **2007**, *19*, 136216–1–136216–26.
[10] C. Adriano, L. Mendonça-Ferreira, E. M. Bittar, P. G. Pagliuso, *J. Appl. Phys.* **2008**, *103*, 07B712–1–07B712–3.
[11] D. A. Joshi, R. Nagalakshmi, S. K. Dhar, A. Thamizhavel, *Phys. Rev. B* **2008**, *77*, 174420–1–174420–10.
[12] D. A. Joshi, A. K. Nigam, S. K. Dhar, A. Thamizhavel, *Phys. Rev. B* **2009**, *80*, 054414–1–054414–9.
[13] C. Adriano, C. Giles, L. N. Coelho, G. A. Faria, P. G. Pagliuso, *Phys. B* **2009**, *404*, 3289–3292.
[14] R. D. Johnson, T. Frawley, P. Manuel, D. D. Khalyavin, C. Adriano, C. Giles, P. G. Pagliuso, P. D. Hatton, *Phys. Rev. B* **2010**, *82*, 104407–1–104407–6.
[15] J. L. Sarrao, L. A. Morales, J. D. Thompson, B. L. Scott, G. R. Stewart, F. Wastin, J. Rebizant, P. Boulet, E. Colineau, G. H. Lander, *Nature* **2002**, *420*, 297–299.
[16] N. J. Curro, T. Caldwell, E. D. Bauer, L. A. Morales, M. J. Graf, Y. Bang, A. V. Balatsky, J. D. Thompson, J. L. Sarrao, *Nature* **2005**, *434*, 622–625.
[17] G. Chen, S. Ohara, M. Hedo, Y. Uwatoko, K. Saito, M. Sarai, I. Sakamoto, *J. Phys. Soc. Jpn.* **2002**, *71*, 2836–2838.
[18] Y. Z. Jia, C. Belin, M. Tillard, L. Lacrois-Orio, D. Zitoun, G. H. Feng, *Inorg. Chem.* **2007**, *46*, 4177–4186.
[19] *Inorganic Crystal Structure Database*, Version 1.7.1, FIZ Karlsruhe, Germany, **2010**.
[20] L. Pauling, *The Nature of the Chemical Bond*, 3rd ed., Cornell University Press, Ithaca, NY, USA, **1960**.
[21] P. Viklund, S. Lidin, P. Berastegui, U. Häussermann, *J. Solid State Chem.* **2002**, *164*, 100–110.
[22] M. A. Zhuravleva, R. J. Pcionek, X. Wang, A. J. Schultz, M. G. Kanatzidis, *Inorg. Chem.* **2003**, *42*, 6412–6424.
[23] Yu. N. Grin', R. E. Gladyshevskii, O. M. Sichevich, V. E. Zavodnik, Ya. P. Yarmolyuk, I. V. Rozhdestvenskaya, *Sov. Phys. Crystallogr.* **1984**, *29*, 528–530; Yu. N. Grin', R. E. Gladyshevskii, O. M. Sichevich, V. E. Zavodnik, Ya. P. Yarmolyuk, I. V. Rozhdestvenskaya, *Transl. Kristallografiya* **1984**, *29*, 893–898.
[24] X. Z. Chen, P. Small, S. Sportouch, M. Zhuravleva, P. Brazis, C. R. Kannewurf, M. G. Kanatzidis, *Chem. Mater.* **2000**, *12*, 2520–2522.
[25] R. T. Macaluso, J. L. Sarrao, N. O. Moreno, P. G. Pagliuso, J. D. Thompson, F. R. Fronczek, M. F. Hundley, A. Malinowski, J. Y. Chan, *Chem. Mater.* **2003**, *15*, 1394–1398.
[26] G. M. Sheldrick, *SHELXTL*, Version 6.12, Bruker AXS Inc., Madison, WI, USA, **2001**.
[27] L. M. Gelato, E. Parthé, *J. Appl. Crystallogr.* **1987**, *20*, 139–143.
[28] J. Rodríguez-Carvajal, *FULLPROF*, Version 4.80, Laboratoire Léon Brillouin (CEA-CNRS), Saclay, France, **2001**.
[29] R. Tank, O. Jepsen, A. Burkhardt, O. K. Andersen, *TB-LMTO-ASA Program*, Version 4.7, Max Planck Institut für Festkörperforschung, Stuttgart, Germany, **1998**.

Received: March 21, 2011
Published Online: June 17, 2011

